This paper describes objective technical results and analysis. Any subjective views or opinions that might be expressed in the paper do not necessarily represent the views of the U.S. Department of Energy or the United States Government.

SAND2018-6526C

Detailed analysis of a waked turbine using a high-resolution scanning lidar

T G Herges[1], J C Berg[1], J T Bryant[1], J R White[1], J A Paquette[1] and B T Naughton[1]

[1]Sandia National Laboratories, Albuquerque, NM, 87185, United States of America

Abstract. Sandia National Laboratories and the National Renewable Energy Laboratory conducted a wake-steering field campaign at the Scaled Wind Farm Technology facility. The campaign included the use of two highly instrumented V27 wind turbines, an upstream met tower, and high-resolution wake measurements of the upstream wind turbine using a customized scanning lidar from the Technical University of Denmark (DTU). The present work investigates the impact of the upstream wake on the downstream turbine power and blade loads as the wake swept across the rotor in various waked conditions. The wake position was tracked using the DTU SpinnerLidar and synchronized to the met tower and turbine sensors. Fully and partially waked conditions reduced the power output and increased the fatigue loading on the downstream wind turbine. Partial wake impingement was found to result in a 10% increase in fatigue loading over the fully waked condition. Rotational sampling of the blade root bending moments revealed that the fatigue damage accrued during full turbine waking, was primarily caused by turbulence within the wake rather than velocity shear, while the partially waked turbine experienced a large 1-per revolution fatigue due to shear. The development of a power to fatigue load metric curve indicated the wake positions where shifting the wake has the most benefit for the waked turbine.

1. Introduction

Wind turbine wakes can significantly influence both the power output and loading of wind turbines within plants, due to the disturbed inflow experienced by downstream turbines. Atmospheric conditions primarily determine the wake propagation to downstream turbines, with stable atmospheric conditions generating more persistent wakes downstream [1]. The IEC 61400-1 Annex D standard accounts for fatigue loading of waked turbines by adding extra turbulence using a method developed by Frandsen [2]. Detailed field campaigns that provide data from highly instrumented wind turbines in various waked conditions along with simultaneous high spatial and temporal resolution wake tracking and velocity deficit measurements have been conducted but remain scarce [3].

In this paper, data from the Sandia National Laboratories (SNL)/US Department of Energy (DOE) Scaled Wind Farm Technology (SWiFT) wind turbines [4] were analyzed to identify the differences in turbine power output and blade loads between fully-waked, partially-waked, and adjacently-waked turbines. The SWiFT facility has well-instrumented meteorological towers and research turbines that include root-bending strain, rotor azimuth position, and nacelle accelerometer measurements all synchronised in time. The upstream wind turbine wake tracking and velocity deficit measurements were coordinated with the downstream turbine sensors using the Technical University of Denmark (DTU) Wind Energy Department custom-built SpinnerLidar [5]. The DTU SpinnerLidar was uniquely capable of measuring the wake at the temporal and spatial resolution required for the experiment. The analysis focused on stable atmospheric conditions in the partial load (Region II) of the production controller, where maximum coefficient of thrust (Ct) occurs.

Sandia National Laboratories is a multimission laboratory managed and operated by National Technology & Engineering Solutions of Sandia, LLC, a wholly owned subsidiary of Honeywell International Inc., for the U.S. Department of Energy's National Nuclear Security Administration under contract DE-NA0003525.

The analysis in this work quantifies the impact of the waked condition on wind turbines. The contribution will improve both high-fidelity modelling and help facilitate future wind turbine and controller design. The study includes the median flap root bending moment, root fatigue loading, and power measurements corresponding to upstream wake position and velocity deficit at the downstream rotor plane. The investigation also includes a loads analysis of the downstream rotor corresponding to different wake conditions [6]. This work provides insights to assess the cost and turbine-life trade-off between power and loads for different waked cases. The data used in this two-turbine waked condition analysis will be made publicly available through the DOE Atmosphere to electron (A2e) Data Archive and Portal (DAP) to support further work by the international research community.

2. Experimental Setup

Sandia National Laboratories operates the SWiFT facility located in Lubbock, Texas. The baseline site instrumentation includes three research wind turbines (WTG) and two meteorological towers (MET) as shown in figure 1a.

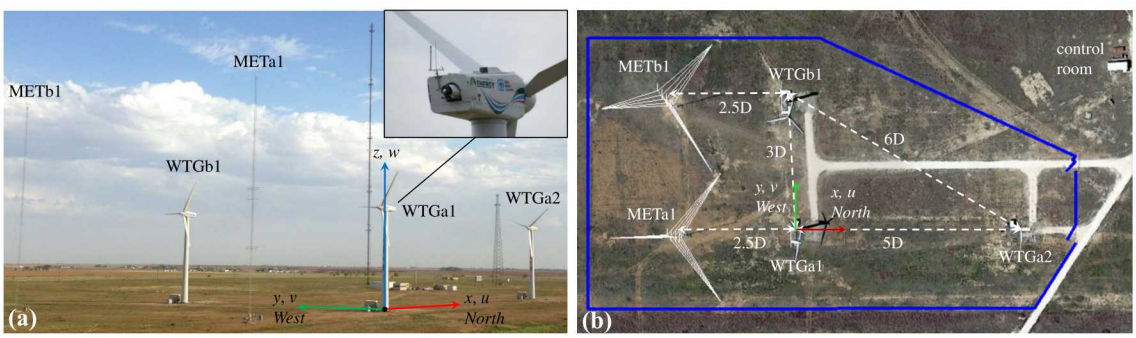

Figure 1. (a) SWiFT site layout and coordinate system with the DTU SpinnerLidar installed in WTGa1 (b) including a top view of the facility layout [4], where D = 27 m.

The layout of the SWiFT facility is seen from an overhead view in figure 1b. The met tower and the two turbines used in this campaign (METa1, WTGa1, and WTGa2) are all aligned with the predominant wind direction at the site, 180 degrees (north is 0 degrees). This configuration allows measurement of the atmospheric inflow with the met tower and measurement of the wake of the WTGa1 turbine using the nacelle-mounted DTU SpinnerLidar. The SWiFT turbines are highly-modified, variable speed, collective pitch Vestas V27 machines with a hub height of 32.1 meters, a rotor diameter of 27 meters, and a maximum power output of 192 kW [4]. The meteorological towers are 59 m tall with a suite of atmospheric sensors as described in Ref. [5]. The entire site is on a fiber optic data acquisition and control network and each WTG and MET are individually synchronised to GPS. Survey locations of the baseline SWiFT site instruments are listed in Ref. [5].

DTU developed the SpinnerLidar to be a turbine mounted lidar for rapid scanning of the wind field in a two-dimensional plane. The SpinnerLidar was uniquely capable of measuring the WTGa1 wind turbine wake at the temporal and spatial resolution required for this experimental campaign. For this experiment, the SpinnerLidar was mounted as shown in figure 2 to point out of the rear of the upwind (WTGa1) turbine nacelle, optimally positioned to capture the full wind turbine wake primarily at five rotor diameters downstream (D = 27 m), near WTGa2. During this portion of the field campaign the SpinnerLidar was angled -15.1° relative to the nacelle centerline to measure the WTGa1 wake through a range of yaw offsets from 0° to 25°. The SpinnerLidar scans the two-dimensional surface of a sphere with an approximately 30° half angle in a fixed rosette pattern, acquiring 984 line-of-sight velocity measurements in 2 seconds [5]. The lidar can also cycle through focus distances with a change in focus distance occurring in the same amount of time as a full scan. The position of the measurement relative to the symmetry axis is calculated from the instantaneous position of the two wedge-shaped prisms. Changes in the orientation of the rotation axis are accounted for using an integrated three-axis accelerometer.

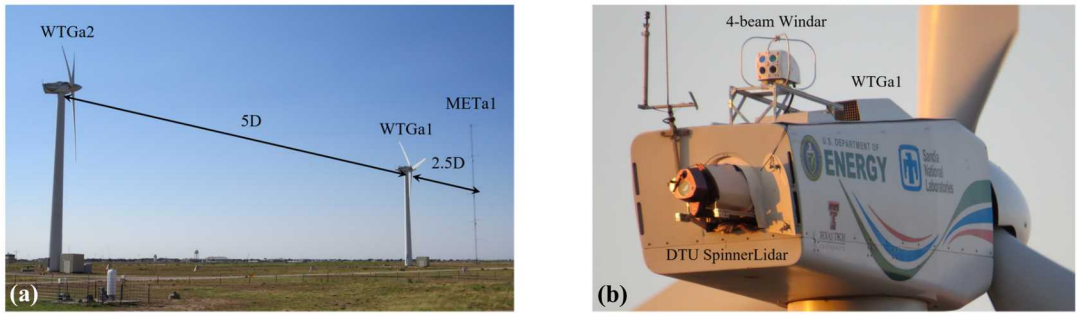

Figure 2. Photo showing the SWiFT instruments that acquired data during the present work: (a) the METa1, WTGa1, and WTGa2 with the spacing labelled, and (b) the installed DTU SpinnerLidar and 4-beam Windar. The 4-beam Windar has a focus distance of 40 m and the data is not included in the current analysis.

Both wind turbines have data acquisition systems mounted in the hub for recording synchronized rotor measurements. For this campaign blade root edge and flap optical Fiber Bragg Grating (FBG) strain sensors were installed and acquired by Micron Optics fiber optic interrogators. As built airfoil profile measurements were taken and precise blade pitch and rotor azimuth calibrations were conducted on the mounted rotor to reduce uncertainty in the orientation of the blade loading. During this campaign, valid data were recorded for one of the blades on both WTGa1 and WTGa2.

3. Experimental Methods and Processing

3.1. SpinnerLidar Measurements and Wake Tracking Method

Wake location tracking is an important quantity of interest for assessing wake steering as a control method along with the impact of the upstream wake on WTGa2 loads and power. The SpinnerLidar measures the line-of-sight velocity from the returned Doppler spectra by calculating the median of frequencies observed within the probe volume above a noise threshold. A number of processing steps were required to extract the wake position from the DTU SpinnerLidar line-of-sight measurements. First, the SpinnerLidar line-of-sight quality assurance and quality control (QA/QC) method removed data points that have a low level of laser signal return relative to the noise threshold as well as points contaminated with laser signal returns from stationary objects due to the introduction of slight object movement from the motion of the laser scan pattern [5, 7]. Second, the location of the measurements in the lidar coordinate system were scaled from an initial normalized frame using the average focus distance over the scan (see Ref. [5]). The orientation and position of the lidar relative to the ground and nacelle was determined using total station theodolite (TST) measurements [8]. The SpinnerLidar had a -15.1° rotation about the z-axis relative to the WTGa1 nacelle centerline during the acquisition of data in this study. The lidar roll and pitch angles were measured by a calibrated 3-axis accelerometer [8], and applied to the data to create the lidar coordinate system. The lidar coordinate system was then transformed into the SWiFT coordinate system (figure 1), where the x direction points North, z is vertical, and y is oriented to create a right-handed coordinate system (pointing West). The origin of the coordinate system was centered along the WTGa1 nacelle yaw rotation axis and located at the base of the turbine foundation. The lidar coordinate system was transformed into the SWiFT site coordinate system by applying a rotation around the z axis with a magnitude corresponding to the yaw heading [7].

A bicubic, smoothing-surface fit was used to interpolate the irregular scan pattern to a regular grid. Next, the wake tracking algorithm was implemented on the line-of-sight velocity regular grid. In the first wake tracking step, the inflow atmospheric boundary layer velocity was subtracted from the measured downstream line-of-sight velocity, revealing any velocity deficit region. The atmospheric boundary layer velocity was estimated as a power law fit of the un-waked edges of the downstream velocity scan. Second, the velocity deficit region from the wind turbine was identified, and the velocity deficit threshold was iteratively determined to match the constraint of an area threshold. In this case, the

area threshold was set to match the rotor area. The area threshold allows the wake tracking method to be robust for a variety of inflow and yaw offset conditions. However, it does not properly capture the expansion of the wake downstream. The wake center was then calculated from the weighted centroid of the velocity deficit within the area of the wake. Finally, the measurement points and wake position in the lidar coordinate system were transformed to the SWiFT coordinate system using rotational coordinate transformations and the angle of the lidar relative to the rotor plane (lidar angle) in addition to the wind turbine yaw heading angle [7].

3.2. Blade Root Strain Measurements

Critical measurements for this work were the FBG strain and temperature sensors within the rotor blade. The FBG sensors were located at the root of the rotor blades on the low-pressure (LP), trailing-edge (TE), high-pressure (HP) and leading-edge (LE) surfaces relative to the global blade coordinate system to measure strain for flap-wise and edge-wise bending. Root temperature sensors were located at the LP and HP positions to measure structural temperature and compensate for thermal strain. In addition, data from the rotor instrumentation, the turbine pitch position, azimuth angle, yaw angle, rotor speed, rotor torque, and rotor power data channels were used for the analysis.

Wind turbine blade operational strain, or total strain, includes an offset in strain typically resulting from the sensor installation process, a varying thermal strain due to the outdoor environmental temperature, a gravitational strain caused by the weight moment of the blade, and the wind loading strains in the flap and edge directions. The quantity of interest for this campaign was the strain caused by wind loading, particularly as it relates to the yaw offset angle of the WTGa1 turbine during wake steering and the waked condition for the WTGa2 turbine. A method was developed to remove the mechanical offset, thermal, and gravitational strains from the total strain, thereby, providing an estimate in the strains exclusively caused by wind loading [6].

3.3. Fatigue Analysis

Fatigue cycles were extracted through Rainflow cycle counting of the edge-wise and flap-wise root bending moment measurements. Fatigue damage was calculated using a power-law equation for fatigue (equation (1)), a simple Goodman relationship for effect of mean moment (equation (2)), and Miner's rule (equation (3)) for damage accumulation [9]. The damage equivalent moment was calculated using equation (4) derived from equation (1) and equation (3) with n = 1e6. Nominal fatigue properties of m = 10 for fiberglass were used. For comparison of the damage equivalent moment (DEM) values, equation (5) was used. All fatigue calculations were performed using MCrunch [10].

$$M = M_u \left(N\right)^{\frac{-1}{m}} \tag{1}$$

$$M_e = \frac{M_a}{\left[1 - \frac{M_m}{M_u}\right]} \tag{2}$$

$$D = \sum \frac{n\left(M_e\right)}{N\left(M_e\right)} \tag{3}$$

$$DEM = M_u \left(\frac{n}{D}\right)^{\frac{-1}{m}} \tag{4}$$

$$\frac{DEM_2}{DEM_1} = \left(\frac{D_1}{D_2}\right)^{\frac{-1}{m}} \tag{5}$$

4. Results

During the wake-steering campaign at the SWiFT site, 12.9 hours of data were collected on July 12th - 13th 2017 where the WTGa2 operated with the WTGa1 wake within a lateral distance of 2D. The DTU SpinnerLidar acquired velocity measurements of the WTGa1 wake with a focus distance of 5D and root strain data were acquired on WTGa2 blade 1. Data collection primarily occurred at night during stable conditions with low turbulence intensities to reduce the impact of the atmosphere on wake

position fluctuations. The atmospheric boundary layer inflow during this period was characterized by the wind speed, turbulence intensity, and power law shear exponent histograms of 0.5-minute bins plotted in figure 3.

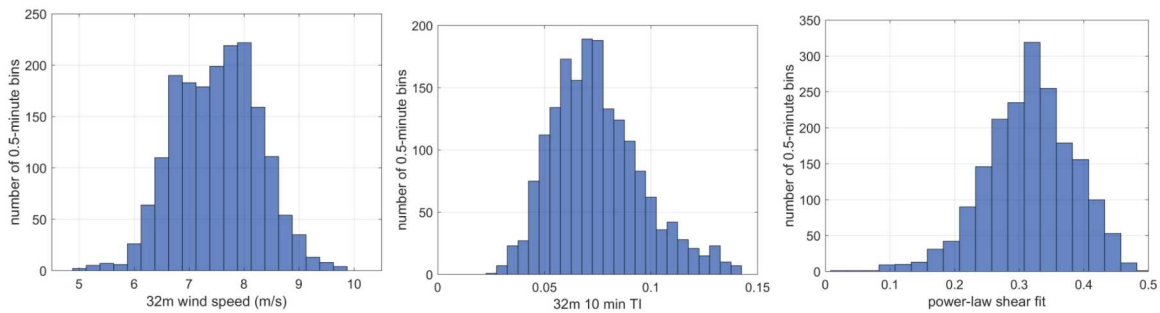

Figure 3. Histogram of 0.5-minute bin inflow conditions as measured by METa1.

The wind direction started each night at 160° and shifted to 190° throughout the evening. As a result, at the start and end of each data collection period, the WTGa1 wake was located west (+*y*) and east (-*y*) of WTGa2, respectively. Throughout this time, different yaw offsets were prescribed to analyze the effect of the upstream WTGa1 wake across the downstream WTGa2 rotor. Thus, the yaw offset set points were not always set to increase power output of the array, but sometimes included steering the wake into the downstream turbine to create various waked conditions on WTGa2. A histogram of the corresponding wake deflection vs yaw offset of WTGa1 in 0.5-minute bins is provided in figure 4. Additional effects of a changing wake shape on WTGa2, beyond wake position due to different yaw offsets, was not included in the current analysis.

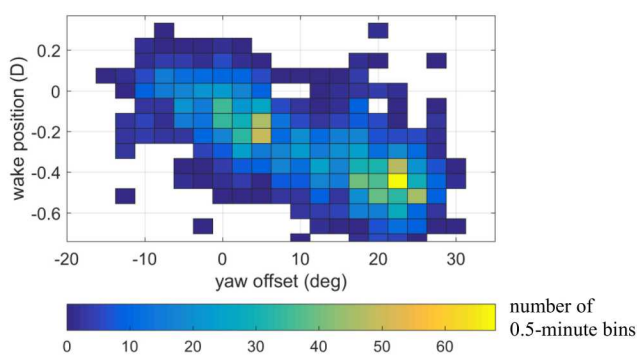

Figure 4. WTGa1 wake deflection vs yaw offset at 5D downstream for the 12.9 hours when WTGa2 was waked by WTGa1.

Figure 5 shows the impact of the WTGa1 wake as measured by the DTU-SpinnerLidar on the WTGA2 power production. Figure 5a displays the measured WTGa1 wake center locations colored with the normalized power output of WTGa2. The normalization values for power and blade root moments were calculated from a fit of the average WTGa2 measurements during non-waked periods for a corresponding met tower hub-height (32 m) wind speed. The locations of the wake center created an arc in the SWiFT coordinate system due to the fixed SpinnerLidar focus distance with different WTGa1 yaw headings. The bin-averaged normalized power versus the position of the WTGa1 wake center are plotted in figure 5b. The results showed a 65% power decrease when WTGa2 was fully waked and a slight (≈0.05%) power increase when the upstream wake edge was located just off the edge of the rotor (figures 6c - 6f). WTGa2 experienced a 30% power loss relative to the non-waked case with a wake center position at the edge of the rotor.

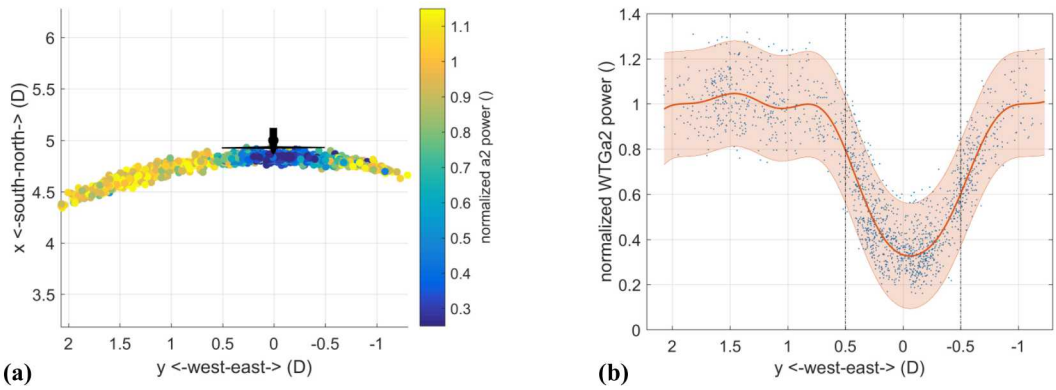

Figure 5. WTGa2 behavior with a DTU SpinnerLidar measured WTGa1 wake center within a lateral distance of 2D using 0.5-minute time bins: (a) measured wake center colored with normalized power, (b) bin-averaged normalized power vs spanwise position of WTGa1 wake (shaded region indicates ±2 σ, standard deviation).

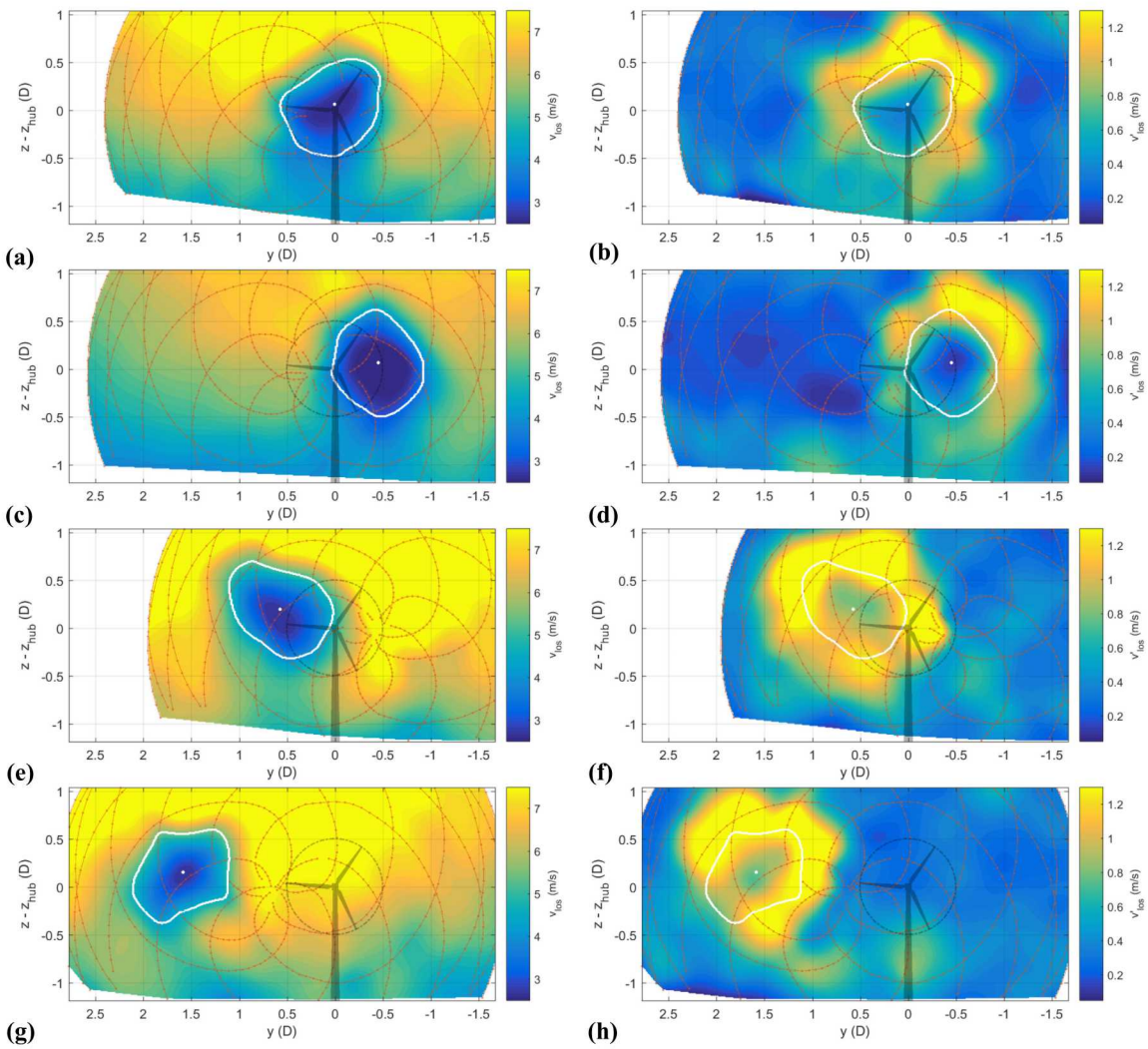

Figure 6. Example SpinnerLidar scans of the line-of-sight velocity (left column) and estimated turbulence (right column) with a wake center position at y = 0 D (0 m) in (a) and (b), y = -0.5 D (-13.5 m) in (c) and (d), y = +0.5 D (+13.5 m) in (e) and (f), and y = +1.5 D (+40 m) in (g) and (h).

Figure 6 provides example scans from the SpinnerLidar corresponding to several wake positions relative to WTGa2. The examples were located at y = 0 D (0 m), ±0.5 D (±13.5 m), and +1.5 D (+40 m) to display the impact of the WTGa1 wake on WTGa2. The scans in figure 6 include the measured line-of-sight velocity and estimated turbulence from the returned continuous-wave lidar Doppler spectra. The turbulence was estimated from the normalized second moment of the Doppler spectra frequencies observed within the continuous-wave lidar probe volume of each scan [11]. The line-of-sight velocity and turbulence helps assess the impact of the WTGa1 wake velocity deficit and turbulent shear layer on the downstream WTGa2 turbine.

Figures 6a and 6b show that when the wake was centered on WTGa2, the turbine did not experience a large velocity change across the rotor but was subjected to the turbulence of the wake shear layer near the outer portion of the rotor. However, the rotor encounters a large velocity change, or shear, across the rotor when the wake was centered at the edge of the rotor (y = ±0.5 D (±13.5 m), figures 6c - 6f) in addition to the turbulence of the shear layer. The turbulence of the wake shear layer does not avoid the inflow of WTGa2 until the wake center reaches a lateral distance of around y = +1.5 D (+40 m) (figures 6g and 6h). The analysis of the WTGa2 blade 1 root strain measurements help to provide insights on the impact of the wake velocity shear and turbulence on the downstream turbine.

Figure 7 displays the per-revolution rotationally sampled frequency content [6] of the root bending flap and edge moments associated with the average wake positions in figure 6. Figure 7 reveals that the fatigue damage accrued during the fully waked condition was primarily caused by turbulence within the wake rather than velocity shear because there were not strong peaks in the frequency decomposition on a per revolution basis. However, broad-spectral noise at higher frequencies was present as compared to the other waked cases, indicating a fatigue load due to turbulence. The partially waked turbine (figures 7b and 7c) incurred large 1-per revolution fatigue loads in both the flap and edge direction due to the shear of the wake velocity deficit. In the adjacently-waked condition (figure 7d), the 1-per revolution load was reduced in addition to the broad-spectral noise due to turbulence. The remaining 1-per revolution load was likely due to the shear of the atmospheric boundary layer.

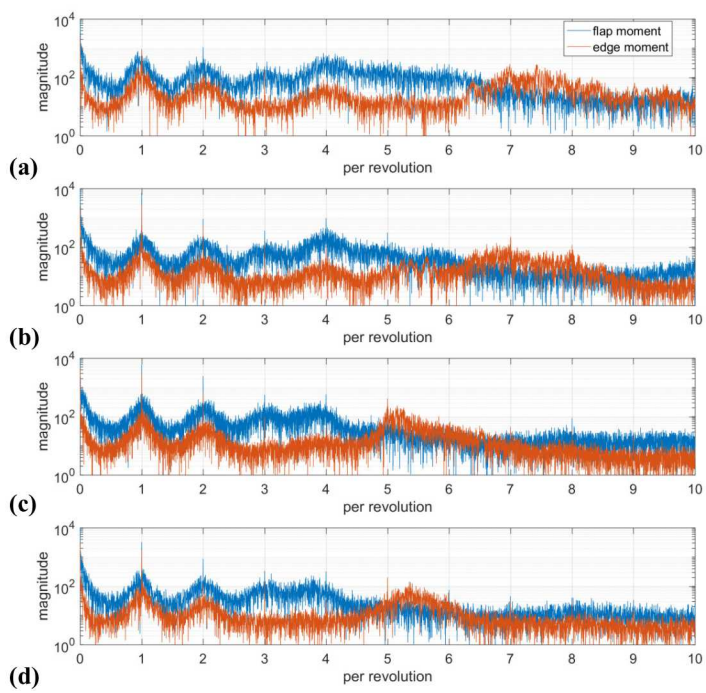

Figure 7. Rotational domain frequency content of the root flap and edge moments associated with an average wake position at (a) y = 0 D (0 m), (b) y = -0.5 D (-13.5 m), (c) y = +0.5 D (+13.5 m), and (d) y = +1.5 D (+40 m). The phase angle corresponding to the rotor azimuth position where the 1-per revolution positive magnitude occurs was (a) 5.0°, (b) 277.9°, (c) 64.5°, and (d) 341.8°.

The WTGa2 blade 1 bin-averaged normalized flap moment contrasted with the WTGa1 wake position is plotted in figure 8a. The corresponding fatigue damage accrued during the 0.5-minute bins is shown in figure 8b as normalized flap DEM. For both quantities, the waked condition was normalized by a fit of the non-waked case with the corresponding METa1 hub-height wind speed. The average flap moment of the waked turbine has a similar profile as the power production with a reduced load when the wake was centered on WTGa2 and an increased load when the velocity deficit of the wake passes the edge of the turbine and the wake shear layer hits the outer portion of the rotor.

The DEM fatigue analysis provides the most insight into how the upstream wake damages WTGa2. WTGa2 accrued a 40% increase in normalized DEM when it was fully waked ($y = 0$ D). However, the DEM increased an additional 10% as the wake moved to the edge of the rotor, on either side. This result indicates that in terms of fatigue damage, a centered wake was preferable. Figure 8b also shows that the DEM did not return to non-waked levels until the wake center reached a lateral position greater than 1.5 D (40 m), where the turbulence from the wake shear layer no longer impinges on the rotor (figure 6h).

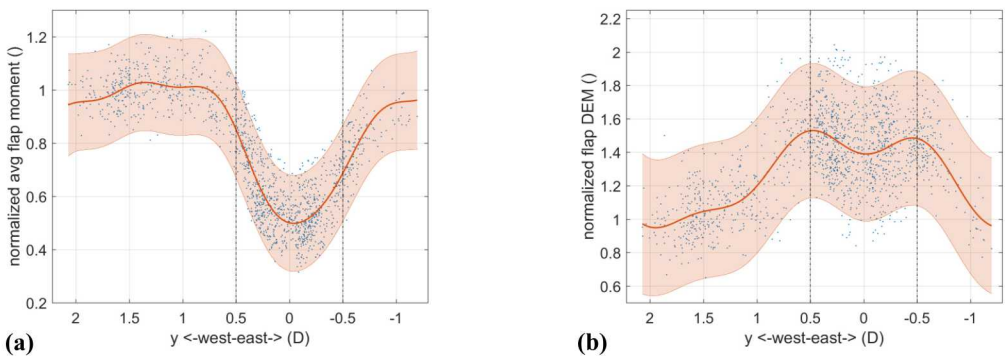

Figure 8. Half-minute bin-averaged normalized blade 1 root flap (a) average moment and (b) DEM, versus spanwise WTGa1 wake position (shaded region indicates ±2 σ, standard deviation).

Figure 9 shows the edge loads in the same format as the flap loads in figure 8. The average edge moment follows the same trends as the average flap moment and power output, with a reduced load while the turbine was fully waked and an increased load when the wake velocity deficit passed near the rotor edge. One difference was that the edge load decreased below the non-waked case when the wake shear layer passes the rotor at $y > 1.5$ D (40 m). The edge fatigue damage was also reduced when the turbine was fully waked but increased when the center of the wake was located at the tip of the rotor. The edge DEM continued to increase as the border of the wake reaches the rotor periphery, near $y = 1.11$ D (30 m). The edge fatigue damaged was reduced when the wake passes the rotor at $y = 1.67$ D (45 m) and returned to the non-waked values as the wake moves farther away from the downstream WTGa2 turbine.

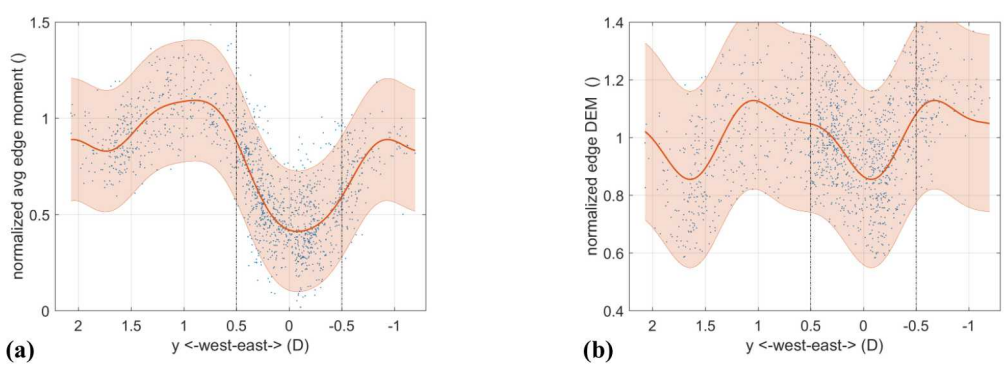

Figure 9. Half-minute bin-averaged normalized blade 1 root edge (a) average moment and (b) DEM, versus spanwise WTGa1 wake position (shaded region indicates ±2 σ, standard deviation).

It should be noted that the overall impact of any measured increase in fatigue loads should be compared to the total overall fatigue loading during operation of a specific turbine within a plant to determine the full effects. The calculation made in this work only covers the effects of fatigue loads at lower wind speeds in Region II operation for a waked turbine with relatively close spacing.

Figure 10 was plotted to compare the increased power production with the flap fatigue damage under waked conditions. Figure 10 shows the 0.5-minute binned normalized power divided by the normalized flap DEM to create a metric for this comparison. The normalized quantities were assumed to have a one-to-one importance and were shifted to align with a value of one at a wake position centered on WTGa2 (y = 0 D) prior to ratioing. This processing step was included to help facilitate the interpretation of the metric results, where a value greater than one indicated the increased normalized power was greater than the accumulated flap fatigue damage under the waked conditions. As a result, figure 10 shows that there was always a benefit to reduce the amount that WTGa2 was waked, even when the wake was located at the edge of the rotor, where the flap DEM was highest. However, there are regions of wake center where it was most beneficial, or important, to try and shift the wake with a control method such as wake steering. Figure 4 shows that WTGa1 has the control authority to shift the wake ≈0.48D (13 m) at 5D with a yaw offset of 25°. Thus, the wake position regions where wake steering was most valuable for the waked turbine are described by the regions of figure 10 where the curve has the largest increase with a 0.5D change in wake center position. When the wind turbine was fully waked, the change in the normalized power to normalized flap DEM was small with a 0.5D deflection in wake position from the rotor center to rotor edge. Conversely, when the wake was located near the edge of the rotor, it would be very beneficial to shift the wake 0.5 D farther from the turbine. The curve also shows the increased benefit to shift the wake away from WTGa2 for wake center positions out to a spanwise distance less than y = 1.5 D (45 m).

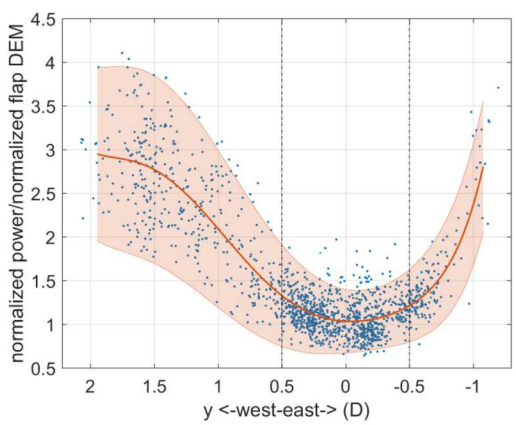

Figure 10. Plot of normalized power divided by normalized flap DEM to create a metric for comparing the power and fatigue damage effects of the wake on WTGa2.

5. Conclusions

The detailed analysis and data in this study help to quantify the impact of the waked condition on wind turbines. As expected, the fully and partially waked conditions reduce the power output and increase the fatigue loading on the downstream wind turbine. The adjacently-waked case creates a power increase with a reduced fatigue loading relative to the fully and partially waked cases. A 10% increase in fatigue loading occurred during partial wake impingement, centered at the rotor tip, relative to when the turbine was fully waked. Rotational sampling of the root bending moments revealed that the fatigue damage accrued during the fully waked condition was primarily caused by turbulence within the shear layer of the wake rather than shear due to the wake velocity deficit, while the partially waked turbine incurred a large 1-per revolution fatigue load due to the shear in the wake. The downstream wind turbine experienced impacts from the upstream wake when the wake center was within a 1.67 D (45 m) spanwise distance of the turbine. A metric created from the ratio of the increased normalized power by

the normalized flap DEM fatigue damage revealed it was always better for the downstream wind turbine to be less waked. However, the metric indicated certain regions where shifting the wake was more beneficial than others with the wake steering control authority of the upstream wind turbine. It was less beneficial to the downstream turbine to shift the wake under fully-waked compared to partially-waked conditions. When the wake was located at the edge of the rotor, it was very beneficial to shift the wake away from the turbine from both a power and fatigue loads perspective.

6. References

[1] Nygaard N G 2014 Wakes in very large wind farms and the effect of neighbouring wind farms *Journal of Physics: Conference Series* **524** 012162

[2] Frandsen S T 2007 Turbulence and turbulence-generated structural loading in wind turbine clusters. (Risø-R-1188(EN)

[3] Machefaux E, Larsen G C, Troldborg N, Hansen K S, Angelou N, Mikkelsen T and Mann J 2016 Investigation of wake interaction using full-scale lidar measurements and large eddy simulation *Wind Energy* **19** 1535-51

[4] Berg J, Bryant J, LeBlanc B, Maniaci D C, Naughton B, Paquette J A, Resor B R, White J and Kroeker D 2014 Scaled Wind Farm Technology Facility Overview. In: *AIAA SciTech 32nd Wind Energy Symposium,*

[5] Herges T G, Maniaci D C, Naughton B T, Mikkelsen T and Sjöholm M 2017 High resolution wind turbine wake measurements with a scanning lidar *Journal of Physics: Conference Series* **854**

[6] White J R, Ennis B L and Herges T G 2018 Estimation of Rotor Loads Due to Wake Steering. In: *AIAA SciTech 2018 Wind Energy Symposium,*

[7] Herges T G, Maniaci D C and Naughton B 2018 Uncertainty Quantification Framework for Wind Turbine Wake Measurements with a Scanning Lidar. In: *AIAA SciTech 2018 Wind Energy Symposium,*

[8] Herges T G, Maniaci D C, Naughton B, Hansen K, Sjöholm M, Angelou N and Mikkelsen T 2017 Scanning Lidar Spatial Calibration and Alignment Method for Wind Turbine Wake Characterization. In: *AIAA SciTech 35th Wind Energy Symposium,*

[9] Sutherland H J 1999 On the Fatigue Anaysis of Wind Turbines. (Sandia National Laboratories: SAND99-0089)

[10] Hayman G and M. Buhl J 2014 MCrunch. (NREL NWTC: https://nwtc.nrel.gov/MCrunch)

[11] Branlard E, Pedersen A T, Mann J, Angelou N, Fischer A, Mikkelsen T, Harris M, Slinger C and Montes B F 2013 Retrieving wind statistics from average spectrum of continuous-wave lidar *Atmos. Meas. Tech.* **6** 1673-83

Acknowledgments

This work was supported by the U.S. Department of Energy under Contract No. DE-AC04-94AL85000 with Sandia National Laboratories, a multimission laboratory managed and operated by National Technology and Engineering Solutions of Sandia, LLC, a wholly owned subsidiary of Honeywell International, Inc., for the U.S. Department of Energy's National Nuclear Security Administration under contract DE-NA-0003525 and the National Renewable Energy Laboratory. Funding for the work was provided by the DOE Office of Energy Efficiency and Renewable Energy, Wind Energy Technologies Office's Wind Energy Atmosphere to Electrons (A2e) Program. In addition to our DOE sponsors, the authors would like to thank the SWiFT support staff, David Mitchell, Miguel Hernandez, and David Martinez. The authors would also like to thank Torben Mikkelsen and Mikael Sjöholm from DTU Wind Energy for their help and expertise installing and using the DTU SpinnerLidar at the SWiFT site in addition to help with data processing discussions. The authors thank Andrew Scholbrock and Donald Baker from the NREL for their support installing the SpinnerLidar at SWiFT. The authors would like to acknowledge Andrew Scholbrock, David Jager, and Jeroen van Dam from NREL for their help with supporting and operating the SWiFT wind turbines, and the NREL colleagues working on the Wake Steering Experiment. An additional thanks to Brandon Ennis for his help with strain measurement data processing.